Inorganic Chemistry

Article

pubs.acs.org/IC

Synthesis, Characterization, and in Vitro Antitumor Activity of Ruthenium(II) Polypyridyl Complexes Tethering EGFR-Inhibiting 4-Anilinoquinazolines

Jun Du,[†] Yan Kang,[†,‡] Yao Zhao,*[,‡] Wei Zheng,[‡] Yang Zhang,[‡] Yu Lin,[‡] Zhaoying Wang,[‡] Yuanyuan Wang,[‡] Qun Luo,[‡] Kui Wu,[‡] and Fuyi Wang*[,‡]

[†]College of Chemistry and Materials Science, Key Laboratory of Functional Molecular Solids, the Ministry of Education, Anhui Laboratory of Molecular-Based Materials, Anhui Normal University, Wuhu 241000, People's Republic of China

[‡]Beijing National Laboratory for Molecular Sciences; CAS Key Laboratory of Analytical Chemistry for Living Biosystems; Beijing Centre for Mass Spectrometry; Institute of Chemistry, Chinese Academy of Sciences, Beijing 100190, People's Republic of China

Supporting Information

ABSTRACT: Ruthenium-based anticancer complexes are promising antitumor agents for their low system toxicity and versatile chemical structures. Epidermal growth factor receptor (EGFR) has been found to be overexpressed in a broad range of tumor cells and is regarded as a drug target in developing novel antitumor drugs. In this work, five ruthenium(II) polypyridyl complexes containing EGFR-inhibiting 4-anilinoquinazoline pharmacophores were synthesized and characterized. These complexes showed both high EGFR-inhibiting activity and strong DNA minor groove-binding activity. In vitro antiproliferation screening demonstrated that the prepared ruthenium complexes are highly cytotoxic against a series of cancer cell lines, in particular non-small-cell lung A549 and human epidermoid carcinoma A431. Fluorescence-activated cell sorting analysis and fluorescence microscopy revealed that the most active complex, **K4**, induced much more late-stage cell apoptosis and necrosis than gefitinib, the first EGFR-targeting antitumor drug in clinical use. These results indicate that the ruthenium(II) polypyridyl complexes bearing EGFR-inhibiting 4-anilinoquinazolines possess highly active dual-targeting anticancer activity and are promising in developing new anticancer agents.

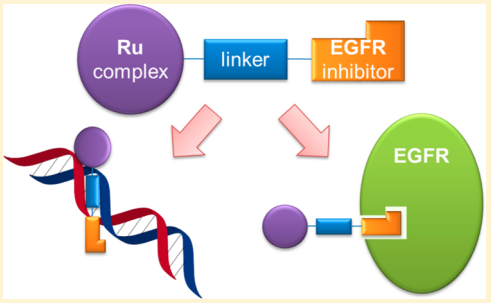

1. INTRODUCTION

Since the discovery of the biological activity of cisplatin in 1965,[1] a series of platinum-based anticancer drugs, such as cisplatin, carboplatin, and oxaliplatin, have been widely used in the clinic for the treatment of ovarian, testicular, bladder, non-small-cell lung cancer, etc. Although great success has been reported using platinum-based anticancer drugs, their application in cancer chemotherapy is limited by multifactorial resistance and serious side effects. These disadvantages promoted the development of other metal-based complexes as novel anticancer agents,[2] such as zinc(II) complexes bearing the active pharmaceutical ingredient curcumin,[3] half-sandwich iridium(III) arene complexes,[4] and potential theranostic agents platinum(II)−gadolinium(III) dinuclear complex.[5] Notably, ruthenium complexes with highly tunable structures, facile construction of octahedral geometry, redox activities, and photochemical properties[6] attracted extensive attention.[7] Particularly, two ruthenium(III) complexes, NAMI-A[8] and KP 1019,[9] have entered clinical trials for various types of cancers or metastasis.[10] Recently, Sadler et al. reported a series of half-sandwich ruthenium(II) arene complexes with potent anticancer activity.[11] Thummel and co-workers reported a series of Ru^{II}-appended pyrenylethynylene complexes that show excellent cytotoxicity against human leukemia cells.[12] Moreover, Ru^{II} polypyridyl complexes have been widely used as DNA binding,[13] cell imaging,[14] and anticancer agents[15] for their facile synthetic chemistry, tunable photophysical/chemical properties, and good water solubility.

Generally, DNA is regarded as one of the major targets for a large group of anticancer drugs.[16] The interactions of metal-based anticancer complexes and DNA have been extensively studied, showing important guiding significance to the research of anticancer drugs.[17] For example, a number of ruthenium-based anticancer complexes with DNA binding[18] or DNA photocleavage[15d] ability have been reported. The Barton and Sauvage groups demonstrated that two Ru^{II} polypyridyl complexes, $[Ru(bpy)_2(dppz)]^{2+}$ and $[Ru(phen)_2(dppz)]^{2+}$ cations (bpy = 2,2′-bipyridine, phen = 1,10-phenanthroline, and dppz = dipyridophenazine), bind to DNA with high affinity with an equilibrium binding constant (K_b) of up to 10^6 M^{-1}.[19] The binding mode of ruthenium anticancer complexes to DNA may include covalent,[18c] (partial) intercalative,[20] electrostatic, and major/minor-groove bonding.[21]

Apart from DNA, enzymes were also recently regarded as an important target of anticancer agents. It has been reported that

Received: February 20, 2016

DOI: 10.1021/acs.inorgchem.6b00309
Inorg. Chem. XXXX, XXX, XXX−XXX

Scheme 1. Synthesis of Ruthenium Complexes K1−K5

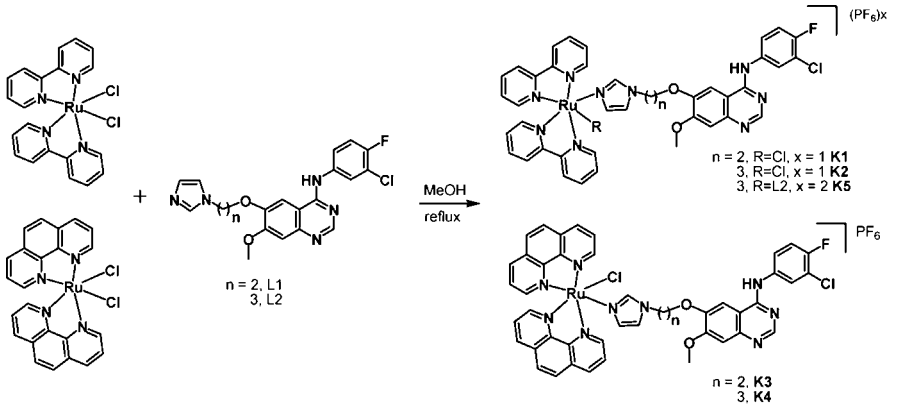

gene mutations leading to overexpression or overactivation of protein tyrosine kinase such as epidermal growth factor receptor (EGFR) are associated with a broad range of malignance, such as non-small-cell lung, ovarian, breast, and squamous cell cancers.[22] EGFR, a transmembrane glycoprotein, can bind to epidermal growth factor (EGF) and is thus activated through dimerization and autophosphorylation of several tyrosine residues.[23] Phosphorylation of the tyrosine residues triggers the downstream signal transduction of a number of intracellular signaling proteins, followed by the activation of a series of physiological processes associated with cell growth, differentiation, apoptosis, and migration.[24] Thus, EGFR and its downstream signaling cascades have been focused on as potential targets for the development of anticancer agents.[25] In the past decades, great effort has been made to develop novel EGFR inhibitors as new anticancer drugs. Among those, molecules containing 4-anilinoquinazolines were found to be highly selective EGFR inhibitors and effective anticancer drugs. This type of antitumor agent exerts its activity by competitive insertion into the ATP-binding pocket of EGFR. A number of 4-anilinoquinazolines derivatives, such as gefitinib and erlotinib, have been available in the clinic for the treatment of non-small-cell lung cancer and squamous carcinoma.[26] Unlike the traditional cytotoxic anticancer drugs, this kind of molecular targeting agent leads to much less toxicity toward normal tissue. However, drawbacks such as noncurative activity are commonly unavoidable.

Since the generation of tumors has been found to be controlled by polygenic factors, dual- or multitargeting treatment of tumors is a promising strategy to improve the efficacy of therapy. For instance, ruthenium anticancer complexes with both potent enzyme-inhibiting and DNA interaction activity have been demonstrated.[27] A platinum-based multitargeting anticancer complex was also reported, which exhibited synergistic DNA binding and anti-inflammatory activity.[28] Multityrosine-kinase inhibitors such as sorafenib[29] and sunitinib[30] are available in the clinic. In our group, a series of dual-targeting ruthenium arene anticancer complexes bearing EGFR-inhibitory pharmacophores have been designed and synthesized,[31] which showed both highly inhibitory potency against EGFR and binding affinity with DNA.

In this work, we rationally designed a series of dual-targeting anticancer compounds by coupling EGFR-inhibitory pharmacophores, 4-anilinoquinazoline derivatives, to noncytotoxic Ru^{II}-polypyridyl subunits. Their structures were characterized and their hydrolysis properties, DNA interactions, EGFR inhibition activities, in vitro antitumor activities, in vitro induction of apoptosis, and distribution in tumor cells were examined. The Ru^{II}-polypyridyl substrates, such as *cis*-[Ru(bpy)$_2$Cl$_2$] and *cis*-[Ru(phen)$_2$Cl$_2$], are nontoxic to cancer cells. However, upon coupling to an EGFR-inhibiting subunit, i.e., 4-anilinoquinazoline pharmacophore, these ruthenium compounds displayed strong antiproliferation activity against cancer cells, and dual-targeting mechanisms of action were found.

2. RESULTS AND DISCUSSION

2.1. Chemistry. The monodentate ligands containing a 4-anilinoquinazoline pharmacophore and an imidazole group for the coordination to Ru were synthesized according to the previous report.[32] The reactions between the ligands L1 and L2 with the ruthenium polypyridyl complexes *cis*-[Ru(bpy)$_2$Cl$_2$] and *cis*-[Ru (phen)$_2$Cl$_2$] afforded complexes *cis*-[Ru(bpy)$_2$(L1)Cl](PF$_6$) (**K1**), *cis*-[Ru(bpy)$_2$(L2)Cl](PF$_6$) (**K2**), *cis*-[Ru(phen)$_2$(L1)Cl](PF$_6$) (**K3**), *cis*-[Ru(phen)$_2$(L2)Cl](PF$_6$) (**K4**), and *cis*-[Ru(bpy)$_2$(L2)$_2$](PF$_6$)$_2$ (**K5**), respectively (Scheme 1). Complexes **K1**−**K4** bear one leaving group, Cl^-, and one monodentate ligand (L1 or L2), while **K5** bears no leaving group but two monodentate ligands (L2). Complexes **K1**−**K4** were synthesized by mixing 1 molar equiv of *cis*-[Ru(bpy)$_2$Cl$_2$] or *cis*-[Ru(phen)$_2$Cl$_2$] with the corresponding ligand L1 or L2 in absolute methanol and refluxing at 80 °C for 10 h under argon in the dark. Complex **K5** was synthesized by refluxing *cis*-[Ru(bpy)$_2$Cl$_2$] and two molar equiv of L2 in absolute methanol at 80 °C for 15 h under argon in the dark. Hexafluorophosphate was added to precipitate the products with satisfactory purification.

Complexes **K1**−**K5** were characterized by ESI-MS, ^{1}H NMR, and ^{13}C NMR spectroscopy and elemental analysis. In the ^{1}H NMR spectra of complexes **K1**−**K5**, the resonances between 10.18 and 7.11 ppm are assignable to the aromatic protons of the 4-(3′ -chloro-4′-fluoroanilino)-7-methoxyquinazoline, imidazole groups, and 2,2′-bipyridine (25H in all) or 1,10′-phenanthroline (25H in all). The singlets ranging from 6.66 to 6.38 ppm (^{1}H) are assignable to the NH of 4-anilinoquinazoline pharmacophores. The typical sharp singlets at 3.7−4.0 ppm (3H) correspond to the CH_3 of the 7-methoxy group of the quinazoline. Complexes **K1**−**K5** have a bis-bipyridine/phenanthroline-coordinated ruthenium moiety conjugated to a derived quinazoline group (two for **K5**) with a flexible C2/C3 chain. The 4-(3′-chloro-4′-fluoroanilino)-7-methoxyquinazoline is the active site of gefitinib, which can target the ATP-binding site of

DOI: 10.1021/acs.inorgchem.6b00309
Inorg. Chem. XXXX, XXX, XXX−XXX

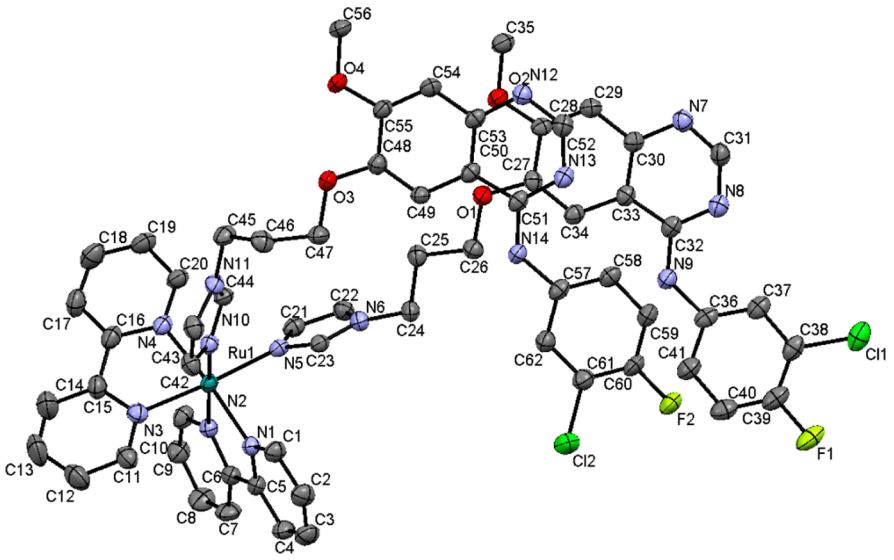

Figure 1. X-ray crystal structure of complex **K5**. The hydrogen atoms, solvents, and PF_6^- anions are omitted for clarity.

EGFR, offering molecules with potential EGFR-inhibiting activity.

Slow diffusion of diethyl ether into a methanol solution of **K5** gave rise to red plate crystals suitable for X-ray diffraction analysis. The X-ray structure and atom numbering are shown in Figure 1; the crystallographic data and the selected bond lengths, angles, and torsion angles are listed in Tables S1 and S2 in the Supporting Information, respectively. As expected, the ruthenium(II) center adopts a distorted octahedral geometry. The bond angles of the bidentate bipyridine ligands with Ru (N(1)−Ru(1)−N(2) and N(3)−Ru(1)−N(4)) are both 79°, smaller than the angle of Ru with two monodentate-derived imidazole ligands in L2 (N(5)−Ru(1)−N(10) = 90°). The bond lengths between Ru and bipyridine or imidazole N-donors are 2.04−2.09 Å, which are very close to the previously reported bond lengths of Ru and N-donors.[31c] Three flexible methylene groups between the quinazoline and the imidazole groups make the 4-anilinoquinazoline pharmacophore and the Ru subunit independent from each other to exert their functions.

2.2. Hydrolysis. Ruthenium complexes containing leaving groups, e.g., chloride, may hydrolyze under physiological conditions. The hydrolysis may affect their chemical properties and interactions with biological molecules. As the derived gefitinib group is crucial for the EGFR-inhibiting activity, the hydrolysis and ligand stability are very important for the complexes in this work. Therefore, HPLC-MS and UV−vis spectroscopy were employed to study the hydrolysis of **K1**−**K5**.

The hydrolysis products of the ruthenium complexes **K1**−**K5** were analyzed by HPLC coupled mass spectrometry. The complexes were incubated in PBS (pH = 7.4, [Cl] = 139.7 mM) at 310 K. After 1 h, an aliquot of the solution was analyzed by HPLC-MS. The HPLC chromatograms and mass spectra for the hydrolysis of **K1**−**K4** are provided in the Supporting Information (Figures S1−S4). Hydrolyzed products with the loss of a Cl^- group for **K1**−**K4** were found. For example, in Figure S4, the HPLC chromatogram of hydrolyzed **K4** displays two signals at 15.5 and 18.2 min, which were identified by ESI-MS to be the aqua adduct of **K4** (**K4**−H_2O) and intact **K4**, respectively. No loss of the derived 4-anilinoquinazoline group (L1 or L2) was found. The chromatogram of HPLC for complex **K5** showed no changes under the same conditions, indicating the hydrolytic inertness of **K5** in PBS (Figure S5). The clean HPLC chromatograms verify the purity of complexes **K1**−**K5** (>90%). The stable bonding of the ligands L1 and L2 maintained the EGFR-inhibiting unit and the ruthenium polypyridyl unit of the complexes, which validates the molecule structures in the following experiments for biological activities.

The hydrolysis reactions of **K1**−**K4** in PBS at 310 K were followed by UV−vis spectroscopy, as shown in Figure 2. The time-dependent changes in the absorbance at selected wavelength of each complex were fitted according to the first-order reaction kinetics to give the hydrolysis rate constants (k) and half-reaction times ($t_{1/2}$), as shown in Table 1. The $t_{1/2}$ of **K1**−**K4** ranges from 9 to 44 min, which are on the same level with the ruthenium arene anticancer complexes bearing EGFR inhibitor pharmacophores (11−33 min).[31a] It is notable that **K2** hydrolyzes faster than **K1**, and **K4** is faster than **K3**, indicating that the bulky 4-anilinoquinazoline group gives rise to steric hindrance to the substitution of the leaving group, and a longer linker can partially counteract the hindrance. Moreover, the hydrolysis rate of **K3** is slower than that of **K1**, and **K4** is slower than **K2**, suggesting that the steric hindrance of the {$Ru(phen)_2$} moiety is higher than that of {$Ru(bpy)_2$} imposing on the chloride group. The complexes **K1**−**K4** generally hydrolyze very fast, so the biological activity research should refer to their hydrolyzed form.

2.3. EGFR Inhibition Activities. The inhibitory activities of the ruthenium complexes **K1**−**K5** and their ligands L1 and L2 toward EGFR were characterized by the enzyme-linked immunosorbent assay (ELISA). The clinically available EGFR inhibitor gefitinib was applied as a reference, with an IC_{50} (half-maximal enzyme activity inhibitory concentration) value of 90 nM. The IC_{50} values of the Ru complexes in this work against EGFR are listed in Table 2, and the concentration-dependent inhibitory curves of **K2**, **K4**, and **K5** are shown in Figure S6. **K1** and **K3** did not pass the preliminary screening, as their IC_{50} values are above 500 nM; thus their curves are not shown. Ligands L1 and L2 are highly potent EGFR inhibitors, as they keep the active site of gefitinib and do not have a steric hindering Ru polypyridyl group. The inhibitory potency of **K2**

DOI: 10.1021/acs.inorgchem.6b00309
Inorg. Chem. XXXX, XXX, XXX−XXX

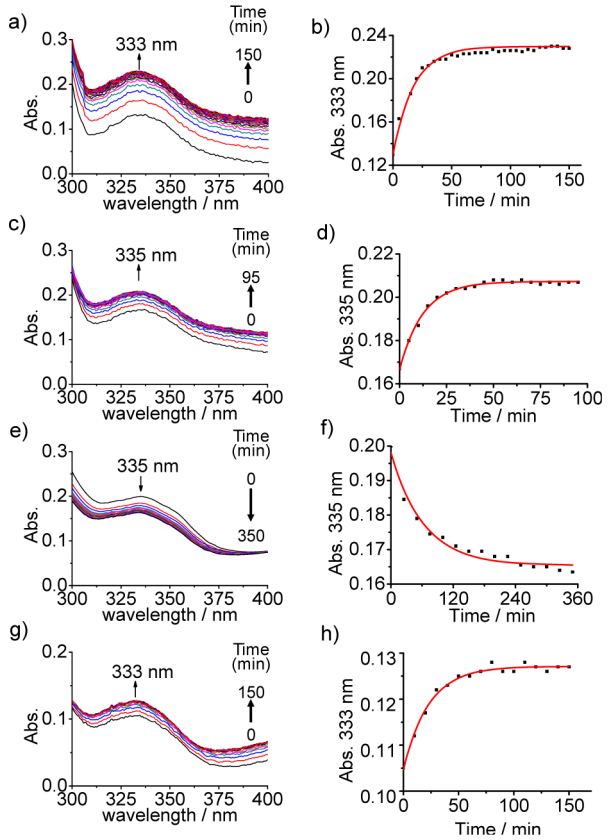

Figure 2. Kinetic study on hydrolysis of complexes **K1**−**K4**. (a, c, e, g) Time-dependent UV−vis absorption spectra for the hydrolysis of **K1**−**K4** (0.01 mM) at 310 K in PBS (pH = 7.4). (b, d, f, h) Time-dependent absorbance at selected wavelength for the hydrolysis of **K1**−**K4** (0.01 mM) at 310 K in PBS (pH = 7.4). The lines are the fittings according to the first-order reaction kinetics.

Table 1. Hydrolysis Rate Constants (k) and Half-Times ($t_{1/2}$) of Complexes K1−K4

	K1	K2	K3	K4
k ($\times 10^{-4}$ s^{-1})	10.3 ± 0.4	13.4 ± 0.6	2.6 ± 0.3	7.3 ± 0.5
$t_{1/2}$ (min)	11.3 ± 0.4	8.6 ± 0.4	43.8 ± 0.9	15.9 ± 1.2

is higher than that of **K1**, and similarly, **K4** is higher than **K3**, which indicates that a longer linker between the 4-anilinoquinazoline moiety and the ruthenium(II) polypyridyl moiety leads to higher EGFR-inhibitory efficiency. These results are in accordance with our previous work,[31a] suggesting that a longer and flexible linker between the ruthenium moiety and the EGFR-inhibiting pharmacophore can lower the steric hindrance for the binding affinity to EGFR. In addition, complex **K5**, bearing two EGFR-inhibiting 4-anilinoquinazoline derivatives, shows the highest activity among **K1**−**K5**, while the EGFR inhibitory efficiencies of complexes **K2** and **K4** are comparable, indicating that, with the same alkyl linker, the different Ru-polypyridyl moieties caused little difference in EGFR-inhibitory activity.

2.4. Competitive DNA-Binding Assays. Ruthenium(II) complexes with distorted octahedral structure are extensively documented to interact with DNA via noncovalent binding, and their cytotoxicity is usually considered to be related to their ability to bind to DNA.[18b] Therefore, studies on the DNA-binding mode of ruthenium antitumor complexes are of great importance. Hence complex **K4**, with the highest overall cytotoxicity, and **K5**, which is structurally different from **K1**−**K4**, are chosen to explore the binding affinity with calf thymus DNA (ctDNA).

Various well-established DNA dyes are employed to decipher the interaction modes of drug and DNA. Ethidium bromide (EB), with a planar structure, is a sensitive fluorescent probe that binds to DNA intercalatively. In aqueous solution, the fluorescent emission of EB is quenched by water molecules, whereas it can be greatly restored upon intercalation within DNA base pairs. However, when another compound competitively replaces EB from the DNA duplex, the fluorescence intensity of the EB−DNA complex may drop, and the binding mode of the new compound toward DNA can be expected to be in the same way as EB.[33]

In this work, first EB was added to the Tris buffer solution (pH = 7.4) of ctDNA, and bright fluorescence at ca. 587 nm was observed. Upon adding complex **K4** to the mixture, the fluorescence intensity centered at ca. 587 nm quenched significantly, as shown in Figure 3a. Similar quenching of fluorescence was observed upon the addition of **K5** to the

Table 2. IC_{50} Values of L1 and L2 and K1−K5 for the Inhibition of EGFR Activity and of the Growth of Selected Cancer Cell Lines

	IC_{50} values								
		A549 (μM)[b]		MCF-7 (μM)[b]		HeLa (μM)[b]		A431 (μM)[b]	
	EGFR (nM)[a]	− EGF	+ EGF	− EGF	+ EGF	− EGF	+ EGF	− EGF	+ EGF
K1	>500	40 ± 4	27 ± 1	31 ± 4	51 ± 1	74 ± 9	42 ± 2	38 ± 6	32 ± 1
K2	371	34 ± 2	28 ± 0.4	35 ± 3	33 ± 1	26 ± 2	28 ± 3	18 ± 1	16 ± 1
K3	>500	34 ± 6	15 ± 2	30 ± 3	18 ± 1	42 ± 7	21 ± 6	23 ± 0.1	16 ± 2
K4	254	25 ± 1	8.6 ± 1	12 ± 1	14 ± 1	11 ± 1	24 ± 8	11 ± 1	13 ± 1
K5	71.6	23 ± 2	13 ± 2	47 ± 2	28 ± 3	50 ± 8	37 ± 1	29 ± 7	27 ± 2
L1	57.4	12 ± 1	13 ± 2	35 ± 2	28 ± 3	19 ± 1	16 ± 1	19 ± 4	13 ± 4
L2	69.6	18 ± 2	13 ± 2	34 ± 2	35 ± 2	47 ± 1	28 ± 2	20 ± 1	15 ± 2
cisplatin	–[c]	10 ± 1	–	13 ± 1	–	12 ± 1	–	5.9 ± 0.4	–
gefitinib	94	16 ± 1	11 ± 1	37 ± 1	23 ± 4	15 ± 1	18 ± 2	–	18 ± 2
cis-$[Ru(bpy)_2Cl_2]$[15e]	–	–	–	–	>200	–	>200	–	–
cis-$[Ru(phen)_2Cl_2]$[15e]	–	–	–	–	>200	–	>200	–	–

[a]The IC_{50} values were determined in the presence of 200 μM ATP and are the average of three independent experiments and expressed as mean ± SD. [b]The cancer cell lines were incubated with each complex for 48 h, and the IC_{50} values are the average of six independent experiments and expressed as mean ± SD. [c]– = not tested.

DOI: 10.1021/acs.inorgchem.6b00309
Inorg. Chem. XXXX, XXX, XXX−XXX

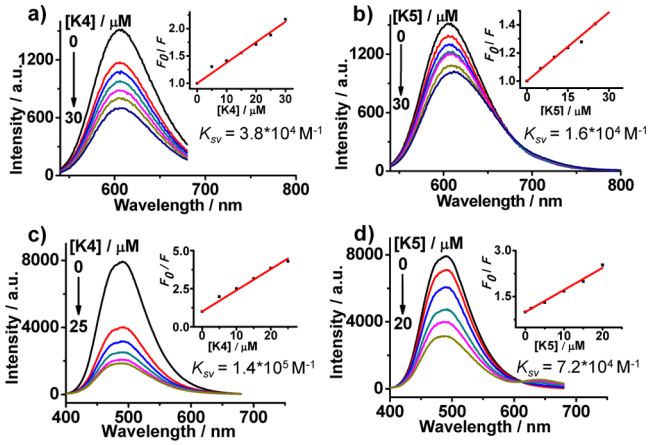

Figure 3. (a, b) Fluorescence titration of the EB−ctDNA complex with **K4** (a) or **K5** (b), λ_{ex} = 525 nm. (c, d) Fluorescence titration of the Hoechst33342−ctDNA complex with **K4** (c) or **K5** (d), λ_{ex} = 370 nm. The insets are the corresponding Stern−Volmer plots for the quenching of fluorescence intensity upon the addition of **K4** or **K5**.

ctDNA−EB mixture (Figure 3b), suggesting that both **K4** and **K5** could replace EB and intercalatively bind to ctDNA.

Another fluorescent probe, Hoechst33342, which binds to DNA through minor groove, was used to further examine the binding mode of the Ru complexes in this work. Because of the quenching by the solvent molecules, Hoechst33342 shows weak fluorescence in Tris buffer solution (pH = 7.4); however, upon binding to ctDNA, the fluorescence intensity at ca. 488 nm increased substantially.[34] The compounds that are able to decrease the fluorescence intensity of DNA−Hoechst33342 complex could be expected to bind to DNA in the minor groove like Hoechst33342. As shown in Figure 3c, upon the addition of **K4**, the fluorescence intensity of the ctDNA−Hoechst33342 mixture quenched sharply. Similar quenching was observed upon the addition of **K5** (Figure 3d), suggesting that both **K4** and **K5** could also replace Hoechst33342 and bind to DNA via the minor groove mode.

The above results suggest that **K4** and **K5** could bind to duplex DNA via both intercalative mode and minor groove mode. To compare the binding affinity of the two modes, we calculated the quenching constant[35] (K_{sv}) for the fluorescence intensity of EB or Hoechst bound to ctDNA by **K4** or **K5** with the Stern−Volmer plot. As shown in the insets of Figure 3a−d, the K_{sv} values of **K4** for EB− and Hoechst−ctDNA complexes are 3.8 × 10^4 and 1.4 × 10^5 M^{-1}, respectively, and the latter is about 2.5-fold higher than the former, suggesting that **K4** tends to interact with DNA via the minor groove mode. The K_{sv} values of **K5** for EB-/Hoechst−ctDNA are 1.6 × 10^4 and 7.2 × 10^4 M^{-1}, respectively, suggesting that **K5** also tends to interact with DNA via the minor groove mode. In addition, it can be concluded that the binding of **K4** to DNA is stronger than that of **K5**.

2.5. Antiproliferation Activity. The antiproliferation activities of the ruthenium(II) complexes **K1**−**K5** and their ligands L1 and L2 were evaluated against four human cancer cell lines, i.e., non-small-cell lung (A549), cervical (HeLa), breast (MCF-7), and squamous (A431) cancer cell lines, by means of the MTT ([3-(4,5-dimethylthiazol-2-yl)-2,5-tetrazolium bromide]) assay. These cancer cells have been reported to overexpress EGFR,[36] and EGF activates this receptor to stimulate the fast growth of the cells and, as a consequence, enhance the effect of the EGFR inhibitors. Therefore, in this work, the antiproliferation assay was carried out both in the absence and in the presence of 100 ng mL^{-1} EGF with 48 h incubation time after addition of the tested ruthenium(II) complexes. In this assay, the clinically available EGFR inhibitor gefitinib[37] and the cytotoxic compound cisplatin were used as positive controls. The IC_{50} values of the tested complexes are shown in Table 2.

All the synthesized ligands and complexes exhibited significant antiproliferation activity against the tested tumor cell lines. As expected, adding EGF reduced their IC_{50} values, in other words, increased the inhibiting potency in almost all cases, except that for complex **K4** against HeLa cells. This suggests that EGF stimulated the repression of EGFR, which is indeed a target of the Ru complexes in this work. Ligands L1 and L2 exhibited overall antiproliferation activity against the tested tumor cell lines similar to gefitinib, simply because they share the same ATP-binding site, and the structure change on the other side is not substantial. Only complex **K4** showed increased overall potency than its corresponding ligand L2, whereas complexes **K1**−**K3** and **K5** did not. Importantly, the cytotoxicity of **K1** and **K3** against MCF-7 or HeLa cells was much stronger than that of their corresponding Ru precursor *cis*-$[Ru(bpy)_2Cl_2]$.[15e] Similarly, **K2** and **K4** are much more cytotoxic than *cis*-$[Ru(phen)_2Cl_2]$.[15e] These results indicate that a synergistic effect may be achieved by coupling the ruthenium moieties with the EGFR-targeting groups.

Among the Ru complexes studied herein, **K4** shows the highest overall antiproliferation activity against the tumor cell lines tested in this work, while **K1** showed the lowest. Notably, the IC_{50} values of **K4** were equivalent to that of cisplatin against HeLa or MCF-7 cell lines in the absence of EGF (Table 2). In the presence of EGF, the IC_{50} values of **K4** against A549, MCF-7, and A431 cells were 8.6, 14, and 13 μM, respectively, which are lower than those of gefitinib, 11, 23, and 18 μM, respectively. In some cases, **K2**, **K3**, and **K5** also exhibited strong inhibition potency against the cancer cell lines. For example, toward MCF-7 cells in the presence of EGF, the IC_{50} values of **K3** and **K5** are 18 and 28 μM, respectively, which are comparable to that of gefitinib (23 μM). In the presence of EGF, the IC_{50} values of **K2** and **K3** against A431 cells are both 16 μM, which are also comparable to that of gefitinib (18 μM).

Moreover, the overall antiproliferation activity of **K2** or **K4** is higher than that of **K1** or **K3**, respectively, but **K1** and **K2** or **K3** and **K4** shared the same Ru moiety and EGFR-targeting group. The only difference between **K1** and **K2** or **K3** and **K4** is the length of the C_n linker (n = 2 for **K1** and **K3**, and n = 3 for **K2** and **K4**). This trend is consistent with their EGFR inhibition activity. These results again indicate that a longer linker between the 4-anilinoquinazoline moiety and the ruthenium(II) polypyridyl moiety can lower the steric hindrance during their interaction with their biological targets, which may contribute to their higher anticancer activities.

The hydrolysis rate and the biological activity for complexes **K1**−**K4** are controversial. On one hand, the overall activity of **K2** or **K4** is higher than that of **K1** or **K3**, respectively, in accordance with the higher hydrolysis rate of **K2** than **K1** and **K4** than **K3**, respectively. On the other hand, although **K1** or **K2** hydrolyzes faster than **K3** or **K4**, respectively, the overall biological activities of **K3** or **K4** are higher than that of **K1** or **K2**, respectively. Therefore, it is suggested that the hydrolysis rate is not the only factor to determine the biological activity,

DOI: 10.1021/acs.inorgchem.6b00309
Inorg. Chem. XXXX, XXX, XXX−XXX

which is also influenced by other factors such as the polypyridyl ligands.

Finally, **K5**, bearing two EGFR-inhibiting 4-anilinoquinazoline pharmacophores, exhibited moderate antiproliferation activity in the absence of EGF against the cancer cells tested compared to **K1**−**K4**. However, in the presence of 100 ng/mL EGF, a substantial decrease of the IC_{50} values was observed toward all the cancer cells tested. Considering the excellent EGFR inhibitory activity of **K5**, even better than gefitinib, it is speculated that **K5** exerts its antiproliferative activities mainly through EGFR inhibition. Similarly, L1 and L2 are also very potent EGFR inhibitors, and their antiproliferation activities are substantially increased upon adding EGF; their activities are also performed through EGFR inhibition.

The Ru complexes in this work displayed higher overall antiproliferation activity than the multitargeting organometallic Ru complexes published previously by our group.[31] However, a dual-targeting platinum complex composed of oxoplatin and aspirin showed more potent anticancer activity against HeLa, MCF-7, HepG2, and A549 cells and, moreover, a lower resistance factor for the A549 cisplatin resistance subcell line.[28]

2.6. Apoptosis Analysis. Since complex **K4** shows the highest overall cytotoxicity against the tested cancer cell lines among all the ruthenium complexes in this work, its ability to induce apoptosis was further explored. Fluorescence microscopy imaging of A549 cells incubated with first complex **4** and then the nuclear staining dye Hoechst33342 was carried out to evaluate the capacity of **K4** to induce apoptotic cell death. As a control in this test, gefitinib is a monofunctional EGFR inhibitor, which exerts its effect mainly by blocking the signaling pathway invoked by autophosphorylation of the EGFR,[26] and is expected to have less capacity to induce apoptotic cell death. As observed from the microscopic images (Figure 4a,b), complex **K4** leads to more apoptotic bodies of A549, characterized by the fragmentation of nuclei with condensed chromatin, than those resulting from gefitinib.

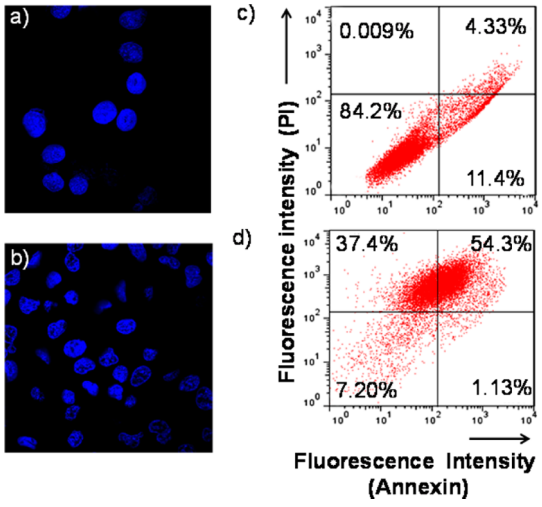

Figure 4. Confocal fluorescent images (left column, a, b) λ_{ex} = 405 nm, λ_{em} = 461 nm. Flow cytometric quantification (right column, c, d) of viable (bottom left quadrant), early-stage apoptotic (bottom right quadrant), late-stage apoptotic (top right quadrant), and necrotic (top left quadrant) A549 cells treated with 50 μM of corresponding complexes in the presence of 10 nM EGF at 310 K for 24 h. The number in each quadrant indicates the respective percentages of total cell populations. Compounds used: (a, c) gefitinib and (b, d) **K4**.

This result indicates that DNA may also be the target of **K4**, which leads to the apoptosis of cancer cells.

Fluorescence-activated cell sorting (FACS) analysis by flow cytometry revealed that complex **K4** (Figure 4d) induced mainly late-stage apoptosis and necrosis and showed much more overall cytotoxicity against A549 than gefitinib (Figure 4c). This result suggests that the coupling of ruthenium(II) polypyridyl precursor *cis*-$[Ru(phen)_2Cl_2]$ and the EGFR-inhibiting 4-anilinoquinazoline pharmacophore offers extraordinary in vitro cytotoxicity toward cancer cell line A549. Furthermore, a positive synergistic effect may be generated via the dual-targeting strategy.

2.7. Distribution of Ruthenium Compounds in HeLa Cells. Time-of-flight secondary mass spectrometry (ToF-SIMS) imaging was employed to analyze the cellular distribution of Ru compounds in cancer cells. The distributions of Ru complexes **K2**−**K4** in single HeLa cells visualized by ToF-SIMS imaging are shown in Figure 5. The green color

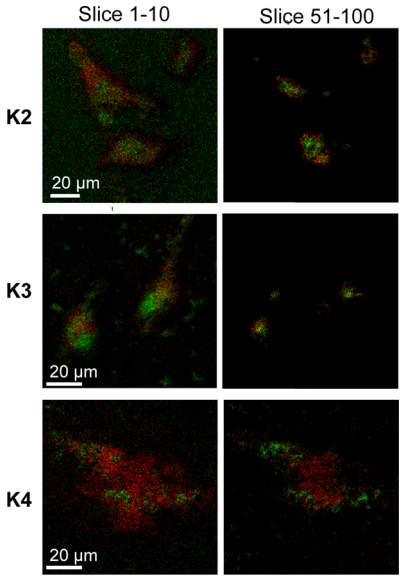

Figure 5. TOF-SIMS images obtained from HeLa cells treated with complex **K2**, **K3**, or **K4** (50 μM). The first column depicts the sum of signals of the 1−10 slices, which corresponds to the surficial level of the cells (membrane), using endogenous phosphocholine fragments at m/z 184.51 as the marker (red color). The second column corresponds to the 51−100 slices, which depicts the deep interior of the cells (nucleus), using endogenous deoxyribose fragments at m/z 81.26 as the marker (red color). The green color indicates the total signal intensity of the Ru-containing fragments for **K2**, m/z 412.91 ($[\mathbf{K2} - L1 - HCl - PF_6]^+$, $C_{20}H_{15}N_4O_2Ru$ requires 413.04) and 449.65 ($[\mathbf{K2} - L1 - PF_6]^+$, $C_{24}H_{15}N_4O_2Ru$ requires 449.01); **K3**, m/z 460.92 ($[\mathbf{K3} - L1 - HCl - PF_6]^+$, $C_{24}H_{15}N_4O_2Ru$ requires 461.04) and 497.66 ($[\mathbf{K3} - L1 - PF_6]^+$, $C_{24}H_{16}N_4O_2ClRu$ requires 497.01; **K4**, m/z 460.89 ($[\mathbf{K4} - L2 - HCl - PF_6]^+$, $C_{24}H_{15}N_4O_2Ru$ requires 461.04) and 497.75 ($[\mathbf{K4} - L2 - PF_6]^+$, $C_{24}H_{16}N_4O_2ClRu$ requires 497.01).

shows the Ru-containing fragment signals of complexes **K2**−**K4** in all the images. The first column depicts the sum of signals of the 1−10 slices, where the red color displays the images of the positive ions at m/z 184, which are the endogenous phosphocholine fragments as a marker of the cell membrane. The second column depicts the sum of signals of the 50−100 slices, where the red color displays the images of the positive ions at m/z 81, which are the endogenous deoxyribose

DOI: 10.1021/acs.inorgchem.6b00309
Inorg. Chem. XXXX, XXX, XXX−XXX

fragments as a cell nucleus marker. All the images depict the overlay of the Ru-containing fragments and the endogenous markers. The SIMS images of individual markers are listed in the Supporting Information (Figures S7−S9). The results show that complexes **K2**−**K4** could penetrate the HeLa cell membrane and go deep inside the cells. Complexes **K2** and **K3** were located not only in the cell membrane but also in the cell nucleus. Whereas for **K4** only a small amount was found in the membrane and the nucleus region, a large amount of **K4** was found in the cytoplasm. Notably, cells treated by complex **K4** were observed to fragment, which may be due to the higher antiproliferation activity of **K4** than that of the other complexes.

Inductively coupled plasma mass spectrometry (ICP-MS) was used to evaluate the binding affinity of Ru complexes to DNA and the membrane proteins in cancer cells. For this purpose, ~10^7 A549 cancer cells were treated with **K4** for 48 h, and then DNA and membrane proteins were extracted, respectively, and the level of ruthenium binding to DNA or membrane proteins was determined by ICP-MS. The level of **K4** was 36.7 ng Ru/mg DNA and 618 ng Ru/mg of membrane proteins. This result supports the SIMS results that complex **K4** was able to accumulate in both the cell membrane and nuclei of the A549 cancer cells, binding to membrane proteins, most likely EGFR, and DNA. This result further verifies that complex **4** can target both membrane proteins and DNA, exhibiting dual-targeting potential, although the Ru uptake of membrane proteins is about 18-fold higher than that of DNA.

3. EXPERIMENTAL SECTION

Materials. $RuCl_3·3H_2O$ (Ru > 36.7%) was purchased from Shenyang Jingke Reagent Co. (China), bipyridine, phenanthrolin, and NH_4PF_6 were from Alfa Aesar, DMSO, cisplatin, and trifluoroacetic acid (TFA) were from Sigma, 1,2-dibromoethane, 1,3-dibromopropane, and imidazole were from Beijing Ouhe Technology Co. (China), and 4-(3-chloro-4′-fluoroanilino)-6-hydroxy-7-methoxyquinazoline (AR grade) was from Shanghai FWD Chemicals Co. (China). *Cis*-$[Ru(bpy)_2Cl_2]$ and *cis*-$[Ru(phen)_2Cl_2]$ were synthesized following methods reported in the literature.[38] Organic solvents including absolute methanol, absolute ethanol, absolute ether, acetonitrile, dichloromethane, and THF were all analytical grade and used directly without further purification. The deionized water used in the experiments was prepared by a Milli-Q system (Millipore, Milford, MA, USA). The protein tyrosine kinase epidermal growth factor receptor and the epidermal growth factor were purchased from Sigma, and other biological agents including the ELISA kits for EGFR inhibitor screening were from Cell Signaling Technology Inc. (USA). ^1H NMR and ^{13}C NMR were recorded on an Avance III 400 spectrometer (Bruker) at 400 MHz for ^1H and 100.6 MHz for ^{13}C.

Synthesis and Characterization. *6-(2-(2-(1H-Imidazol-1-yl)-ethoxy)-4-(3′-chloro-4′-fluoroanilino)-7-methoxyquinazoline (L1).* Compound L1 was synthesized following a method reported in the literature[31a,32] with minor modifications. 4-(3′-Chloro-4′-fluoroanilino)-6-hydroxy-7-methoxyquinazoline (8.0 g, 25 mmol) and potassium carbonate (18.0 g, 115.9 mmol) were mixed in DMF (300 mL). Then 1,2-dibromoethane (8 mL, 92.4 mmol) was added, and the resulting mixture was heated at 80 °C for 8 h. After cooling to room temperature, the mixture was filtered under vacuum, and the filtrate was collected. Then the solvent was evaporated in a vacuum, and the residue was recrystallized from ethanol. The yellow crude product was further purified by flash chromatography on silica gel using ethyl acetate/petroleum (5:2) as eluent to give 4-(3′-chloro-4′-fluoroanilino)-6-(2-bromoethoxy)-7-methoxyquinazoline (L1′) as white powder (4.8 g, 45%). Imidazole (355 mg, 5.2 mmol), tetrabutyl ammonium bromide (TBAB) (41.3 mg, 0.133 mmol), and NaOH (s) (624 mg, 15.6 mmol) were mixed in acetonitrile (60 mL). The reaction mixture was heated to 90 °C and refluxed for 1 h; then compound L1′ (1.33 g, 3.12 mmol) was added, and the mixture was refluxed for 5 h. After cooling to room temperature, the mixture was filtered in a vacuum and the filtrate was collected and evaporated to give a yellow oil. Then deionized water (50 mL) and ethyl acetate (50 mL) were added. A light yellow solid appeared between the water phase and ethyl acetate phase after ultrasonic vibration for 5 min and standing for 1 h, and the mixture was filtered under vacuum and washed with water and ethyl acetate to give L1 as light yellow powder (0.8 g, 62%). Mp: 259−261 °C. Ligand L1 is slightly soluble in DMSO-d_6, but the solubility is too low to allow for ^{13}C NMR measurements. ESI-MS: m/z 414.2 ($[M + H]^+$ requires 414.1). ^1H NMR (400 MHz, DMSO-d_6, TMS): δ_H (ppm) 9.53 (s, 1H), 8.47 (s, 1H), 8.06 (dd, J_1 = 4.0 Hz, J_2 = 2.4 Hz, 1H), 7.77 (s, 1H), 7.74−7.71 (m, 2H), 7.41 (t, $J_1 = J_2$ = 9.2 Hz, 1H), 7.29 (s, 1H), 7.19 (s, 1H), 6.91 (s, 1H), 4.48 (t, $J_1 = J_2$ = 5.2 Hz, 2H), 4.38 (t, J_1 = 4.8 Hz, J_2 = 5.6 Hz, 2H), 3.93 (s, 3H). Anal. (%) Calcd for $C_{20}H_{17}ClFN_5O_2$: C, 58.05; H, 4.14; N, 16.9. Found: C, 58.04; H, 4.20; N, 16.32.

6-(2-(3-(1H-Imidazol-1-yl) propoxy)-4-(3′-chloro-4′-fluoroanilino)-7-methoxyquinazoline (L2). 4-(3′-Chloro-4′-fluoroanilino)-6-hydroxy-7-methoxyquinazoline (12.0 mg, 37.6 mmol) and potassium carbonate (24.0 mg, 173.6 mmol) were mixed in acetone (500 mL). Then 1,3-dibromopropane (15.2 mL, 149.2 mmol) was added, and the resulting mixture was refluxed for 10 h. After cooling to room temperature, the mixture was filtered under vacuum and the filtrate was collected. Then the solvent was evaporated under vacuum, and the residue was recrystallized from ethanol. The yellow residue was further purified by flash chromatography on silica gel using ethyl acetate/petroleum (3:1) as eluent to give 4-(3′-chloro-4′-fluoroanilino)-6-(2-bromopropoxy)-7-methoxyquinazoline (L2′) as white powder (6.0 g, 36%). Imidazole (516 mg, 7.6 mmol), TBAB, (60 mg, 0.2 mmol), and NaOH (s) (908 mg, 22.6 mmol) were mixed in acetonitrile (100 mL). The reaction mixture was heated to 90 °C and refluxed for 1 h; then compound L2′ (2.0 g, 4.54 mmol) was added and the mixture was refluxed for 5 h. After cooling to room temperature, the mixture was filtered under vacuum and the filtrate was collected and evaporated to give a yellow oil. Then water (80 mL) and ethyl acetate (80 mL) were added. A light yellow solid appeared between the water phase and the ethyl acetate phase after ultrasonic vibration for 5 min and standing for 1 h, and the mixture was filtered under vacuum and washed with water and ethyl acetate to give L2 as a light yellow powder (1.4 g, 72%). Mp: 201−203 °C. ESI-MS: m/z 428.2 ($[M + H]^+$ requires 428.1). ^1H NMR (400 MHz, DMSO-d_6, TMS): δ_H (ppm) 9.51 (s, 1H), 8.50 (s, 1H), 8.10 (dd, J_1 = 2.4 Hz, J_2 = 2.8 Hz, 1H), 7.79−7.75 (m, 2H), 7.64 (s, 1H), 7.43 (t, $J_1 = J_2$ = 9.2 Hz, 1H), 7.22 (s, 2H), 6.91 (s, 1H), 4.20 (t, $J_1 = J_2$ = 6.8 Hz, 2H), 4.08 (t, $J_1 = J_2$ = 6.0 Hz, 2H), 3.97(s, 3H), 2.33−2.27(m, 2H). ^{13}C NMR (DMSO-d_6,400 MHz, TMS): δ_C (ppm) 156.49, 155.01, 153.20, 148.51, 147.61, 137.84, 129.05, 123.91, 122.70, 119.84, 119.33, 119.15, 117.04, 116.83, 109.20, 107.88, 103.47, 66.17, 56.41, 43.39, 30.55. Anal. (%) Calcd for $C_{21}H_{19}ClFN_5O_2·H_2O$: C, 56.57; H, 4.75; N, 15.71. Found: C, 56.51; H, 4.61; N, 15.46.

Synthesis and Characterization of $[(N^{\wedge}N)_2Ru(L)Cl]PF_6$ (K1−K5). *General Procedure.* The five complexes **K1**−**K5** were prepared following the methods below. The 4-anilinoquinazoline derivative L1 or L2 (0.1 mmol) and corresponding *cis*-$[(N^{\wedge}N)_2Ru(Cl)_2]$ (*cis*-$[Ru(bpy)_2Cl_2]$ or *cis*-$[Ru(phen)_2Cl_2]$, 0.1 mmol for **K1**−**K4**, 0.2 mmol for **K5**) were dissolved in methanol (60 mL), and the mixture was refluxed under Ar in the dark until the solution became clear. After cooling to room temperature, the solution was filtered and excess ammonium hexafluorophosphate (0.3 mmol for **K1**−**K4**, 0.4 mmol for **K5**) was added to this mixture and further stirred for 2 h at 318 K to precipitate the product. The solid collected after filtration was washed with excess methanol and recrystallized from MeOH to give the product. Complexes **K1**−**K5** were characterized by ESI-MS, ^1H NMR spectroscopy, ^{13}C NMR spectroscopy, and elemental analysis, as shown below.

K1: MS (m/z): 431.571 ($[M - PF_6 + H]^{2+}$ requires 431.562). ^1H NMR (DMSO-d_6, 400 MHz): δ (ppm) 9.86 (d, J = 5.2 Hz, 1H), 9.59 (s, 1H), 8.73 (d, J = 8 Hz, 1H), 8.64−8.61 (m, 2H), 8.56 (d, J = 8 Hz, 2H), 8.39 (d, J = 5.2 Hz, 1H), 8.10 (t, J_1 = 8.4 Hz, J_2 = 8 Hz, 3H), 8.04 (t, J_1 = 7.6 Hz, J_2 = 7.2 Hz, 1H), 7.89−7.83 (m, 3H), 7.77−7.72 (m, 3H), 7.55−7.50 (m, 2H), 7.46 (t, $J_1 = J_2$ = 9.2 Hz, 1H), 7.37 (s, 1H),

DOI: 10.1021/acs.inorgchem.6b00309
Inorg. Chem. XXXX, XXX, XXX−XXX

7.28 (dd, $J_1 = J_2 = 7.2$ Hz, 2H), 7.23 (s, 1H), 6.41 (s, 1H), 4.54 (t, $J_1 = J_2 = 5.6$ Hz, 2H), 4.36 (t, $J_1 = J_2 = 3.6$ Hz, 2H), 3.88 (s, 3H). Anal. (%) Calcd for $C_{40}H_{37}Cl_2F_7N_9O_4PRu$ (M + $2H_2O$): C, 46.03; H, 3.57; N, 12.08. Found: C, 46.06; H, 3.35; N, 12.29.

K2: MS (m/z): 420.591 ($[M - PF_6 - Cl]^{2+}$ requires 420.582). ^{1}H NMR (MeOD, 400 MHz): δ (ppm) 9.81 (d, J = 5.2 Hz, 1H), 8.44−8.36 (m, 4H), 8.30 (dd, $J_1 = J_2 = 8$ Hz, 2H), 8.11 (s, 1H), 7.97 (d, J = 1.2 Hz, 1H), 7.89−7.82 (m, 2H), 7.77−7.67 (m, 5H), 7.62 (s, 1H), 7.59(d, J = 5.6 Hz, 1H), 7.49 (t, $J_1 = J_2 = 6.4$ Hz, 1H), 7.35 (t, $J_1 = J_2 = 6.4$ Hz, 1H), 7.20−7.11 (m, 5H), 6.44 (s, 1H), 4.32−4.23 (m, 2H), 3.97 (m, 3H), 3.93−3.86 (m, 2H), 2.28−2.20 (m, 2H). Anal. (%) Calcd for $C_{41}H_{40}Cl_2F_7N_9O_{4.5}PRu$ (M + $2.5H_2O$): C, 46.16; H, 3.78; N, 11.82. Found: C, 46.11; H, 3.77; N, 11.84.

K3: MALDI-TOF-MS (m/z): 437.576 ($[M - PF_6 - Cl]^{2+}$ requires 437.574). ^{1}H NMR (DMSO-d_6, 400 MHz): δ (ppm) 10.18 (d, J = 4.8 Hz, 1H), 9.43 (s, 1H), 8.85 (d, J = 4.8 Hz, 1H), 8.71(dd, J_1 = 8 Hz, J_2 = 8.4 Hz, 2H), 8.52 (s, 1H), 8.40 (dd, $J_1 = J_2 = 8$ Hz, 2H), 8.31 (d, J = 8.8 Hz, 1H), 8.25−8.13 (m, 5 H), 8.07 (dd, $J_1 = J_2 = 2.4$ Hz, 1H), 8.00 (d, J = 5.2 Hz, 1H), 7.92 (dd, $J_1 = J_2 = 5.2$ Hz, 1H), 7.76−7.72 (m, 3H), 7.49−7.39 (m, 3H), 7.29 (s, 1H), 7.21 (s, 1H), 6.44 (s, 1H), 4.52−4.45 (m, 2H), 4.36−4.27 (m, 2H), 3.83 (s, 3H). Anal. (%) Calcd for $C_{44}H_{36}Cl_2F_7N_9O_{3.5}PRu$ (M + $1.5H_2O$): C, 48.81; H, 3.35; N, 11.64. Found: C, 48.98; H, 3.36; N, 11.38.

K4: MALDI-TOF-MS (m/z): 462.595 ($[M - PF_6 + H]^{2+}$ requires 462.571). ^{1}H NMR (DMSO-d_6, 400 MHz): δ (ppm) 10.04 (d, J = 4.8 Hz, 1H), 9.43 (s, 1H), 8.81 (d, J = 4.9 Hz, 1H), 8.62 (d, J = 8.0 Hz, 1H), 8.54 (d, J = 8.0 Hz, 1H), 8.50 (s, 1H), 8.34 (d, J = 7.9 Hz, 1H), 8.28−8.23 (m, 2H), 8.12 (t, $J_1 = J_2 = 8.4$ Hz, 2H), 8.06−7.99 (m, 3H), 7.94−7.92 (m, 2H), 7.90−7.88 (m, 1H), 7.74−7.70 (m, 1H), 7.65 (d, J = 6.4 Hz, 2H), 7.40−7.36 (m, 3H), 7.22 (s, 1H), 7.16 (s, 1H), 6.46 (s, 1H), 4.09 (t, J_1 = 6.8 Hz, J_2 = 6.4 Hz, 2H), 3.88−3.83 (m, 5H), 2.17−2.11(m, 2H). Anal. (%) Calcd for $C_{45}H_{39}Cl_2F_7N_9O_4PRu$ (M + $2H_2O$): C, 48.88; H, 3.55; N, 11.40. Found: C, 49.02; H, 3.40; N, 11.36.

K5: MALDI-TOF-MS (m/z): 634.138 ($[M - 2PF_6]^{2+}$ requires 634.143). ^{1}H NMR (DMSO-d_6, 400 MHz): δ (ppm) 9.43 (s, 2H), 8.85 (d, J = 5.2 Hz, 2H), 8.45 (d, J = 8 Hz, 4H), 8.35 (d, J = 8.2 Hz, 2H), 8.04 (dd, $J_1 = J_2 = 2.4$ Hz, 2H), 7.94 (t, $J_1 = J_2 = 7.6$ Hz, 2H), 7.77−7.69 (m, 8 H), 7.64 (s, 2H), 7.59 (t, $J_1 = J_2 = 6.4$ Hz, 2H), 7.39 (t, $J_1 = J_2 = 8.8$ Hz, 2H), 7.29−7.25 (m, 4H), 7.16 (s, 2H), 6.66 (s, 2H), 4.05 (t, $J_1 = J_2 = 6.8$ Hz, 4H), 3.90−3.86 (m, 4H), 3.83 (s, 6H), 2.14−2.11 (m, 4H). Anal. (%) Calcd for $C_{62}H_{58}Cl_2F_{14}N_{14}O_6P_2Ru$ (M + $2H_2O$): C, 46.68; H, 3.66; N, 12.29. Found: C, 46.72; H, 3.47; N, 12.20.

X-ray Crystallography. A crystal of **K5** suitable for single-crystal X-ray diffraction with a size of 0.21 × 0.17 × 0.04 mm^3 was selected. Data were collected on an MM007-HF CCD (Saturn 724+) diffractometer in ω scans with confocal-monochromated Mo Kα (λ = 0.710 73 Å) radiation. The structure was refined with full-matrix least-squares on F^2 using the SHELXL (Sheldrick, 2013) programs. Crystal parameters and details of the data collection and refinement are shown in Table S1. Selected bond lengths (Å) and bond angles (°) are shown in Table S2.

Electrospray Ionization Mass Spectroscopy (ESI-MS). The positive-ion ESI mass spectra for the hydrolytic products were obtained with a Xevo G2 Q-TOF (Waters USA), which was equipped with a Masslynx (ver. 4.0) data processing system for analysis and postprocessing. The spray voltage and the cone voltage were 3.5 kV and 5 V, respectively. The desolvation temperature was 623 K, and the source temperature 373 K. Nitrogen was used as both cone gas and desolvation gas with a flow rate of 50 and 800 L h^{-1}, respectively. The spectra were acquired in the range 200−2000 m/z.

Hydrolysis of Complexes. The kinetic studies on the hydrolysis of complexes **K1**−**K5** were carried out employing a UV-2550 spectrometer (Shimadzu, Japan). First, the tested complex was dissolved in DMSO at a concentration of 2 mM, an aliquot (15 μL) of the DMSO solution was then added to 2985 μL of PBS (pH = 7.4) in a quartz cuvette, and the UV−vis spectra of the mixture were immediately recorded by scanning over the wavelength ranging from 200−800 nm at 5 min intervals at 37 °C. The wavelength corresponding to the maximum absorbing changes of each hydrolysis reaction was selected for measurement of the rate constant. The same procedures as described above were used to prepare the samples for the kinetic study. The absorbance at selected wavelength for each complex was recorded at 5 min intervals. The time-dependent absorbance was fitted using Origin 8.0 (OriginLab Corporation, USA) to give the first-order rate constant k, and the half-reaction time $t_{1/2}$ was calculated by the following formula:

$$A = Ce^{-kt} + A_0$$

$$t_{1/2} = \ln 2/k$$

where A is the absorbance and A_0 and C are constants.

To identify the hydrolysis products, the samples were prepared by diluting a DMSO solution of the each complex (10 mM) with PBS (pH = 7.4) to 1 mM. The solution was incubated at 310 K for 1 h, an aliquot of which was then analyzed by HPLC coupled with ESI-MS. An Agilent 1200 series quaternary pump and a Rheodyne sample injector with a 20 μL loop, an Agilent 1200 series UV−vis DAD detector, and Chemstation data processing system were used. The mobile phase solvent A was water containing 0.1% TFA, and solvent B was acetonitrile containing 0.1% TFA. The separation of hydrolytic adducts of the ruthenium complexes was carried out on an Agilent Eclipse XDB-C18 reversed-phase column (4.6 × 150 mm, 5 μm). The gradient B was 10% to 60% from 0 to 25 min, 60% to 80% for 3 min, and 80% for 2 min.

In Vitro Antiproliferation Assays. The human lung adenocarcinoma A549, human cervical cancer HeLa, human breast cancer MCF-7, and human epidermoid carcinoma A431 cell lines were obtained from the Centre for Cell Resource of Peking Union Medical College Hospital and were maintained in DMEM medium supplemented 90% DMEM (Invitrogen, USA) + 10% fetal bovine serum (Invitrogen, USA) + 1% penicillin−streptomycin (Invitrogen, USA). On request, an aliquot of 100 ng mL^{-1} epidermal growth factor (Sigma, USA) was added into the media. The cells were grown at 310 K in a humidified atmosphere containing 5% CO_2 for 2−3 days prior to screening experiments.

The IC_{50} values were determined by the MTT assay. Cells were counted by a Luna automated counter (Logos Biosystems, Korea) and were plated at a density of 5000 cells/well (A549), 6500 cells/well (HeLa), 8000 cells/well (MCF-7), and 8000 cells/well (A431), respectively, in 100 μL of media in 96-well plates and grew in the absence or the presence of EGF for 24 h. The stock solutions (10 mM, except for cisplatin (1 mM)) of all tested complexes were made up fresh in DMSO before diluted down in media to give the required concentration for addition to the cells. For each ruthenium complex, eight different concentrations were prepared from the stock solution by diluting with the cell culture medium prior to use, and the concentration of DMSO was kept 1% in all dilutions. Cells were then exposed to each tested complex at various concentrations for 48 h. Then the drug media was discarded and washed three times with PBS, and 100 μL of complete medium containing MTT (0.5 mg/mL) was added to each well and incubated at 310 K for 4 h. The MTT media was removed, and 100 μL of DMSO was added to each well to dissolve the crystals at room temperature for 10 min. Optical density (OD) for each well was measured using a microplate reader (SpectraMax M5, Molecular Devices Corporation) at the wavelength of 570 nm. The inhibition rate (IR) was calculated based on the following equation:

$$IR(\%) = [1 - (OD_{complex} - OD_{blank})/(OD_{control} - OD_{blank})] \times 100\%$$

All values of IR reported were averages of six independent experiments and expressed as mean ± SD (standard deviation).

Competitive Displacement of DNA Binding Assays. The EB displacement assay was done in Tris buffer solution (5 mM, pH = 7.4). The concentration of ctDNA and EB was kept at 20 and 200 μM, respectively, in the solution, which was titrated with varying concentrations of **K4** or **K5** from 0 to 100 μM. The ctDNA-EB complex was excited at 525 nm, and the emission spectra were

DOI: 10.1021/acs.inorgchem.6b00309
Inorg. Chem. XXXX, XXX, XXX−XXX

recorded from 535 to 800 nm. Emission spectra were obtained on a Hitachi F-4500 fluorescence spectrophotometer (Japan). Measurement parameters: PMT voltage, 700 V; EX slit, 10.0 nm; EM slit, 10.0 nm.

The Hoechst33342 displacement assay was also done in Tris buffer solution (5 mM, pH = 7.4). The concentration of ctDNA and Hoechst33342 was kept at 20 and 200 μM, respectively, in the solution, which was titrated with varying concentrations of competing complexes from 0 to 100 μM. The ctDNA−Hoechst33342 complex was excited at 370 nm, and emission spectra were recorded from 400 to 680 nm. Measurement parameters: PMT voltage, 700 V; EX slit, 5.0 nm; EM slit, 5.0 nm.

The Stern−Volmer constant (K_{sv}) was used to evaluate the fluorescence quenching efficiency. The classical Stern−Volmer equation is $F_0/F = 1 + K_{sv}[Q]$, where F_0 and F are the fluorescence intensities before and after the addition of the quencher, respectively, [Q] is the concentration of the quencher, and K_{sv} is the quenching constant.

Enzyme-Linked Immunosorbent Assay (ELISA). ELISA, a widely used in vitro screening method for enzyme inhibitors, was applied to characterize the inhibition potency of ruthenium(II) polypyridyl complexes containing 4-anilinoquinazoline ligands toward EGFR. The receptor tyrosine kinase solution in 50% glycerol, containing 50 mM HEPES (pH = 7.6), 150 mM NaCl, 0.1% Triton, and 1 mM dithiothreitol (DTT), was purchased from Sigma; phosphotyrosine mouse mAb (P-Tyr-100), signal transduction protein (Tyr66) biotinylated peptide, adenosine-triphosphate (ATP), and dl-DTT HTScan tyrosine kinase buffer (4×) were purchased from Cell Signaling Company; HRP-labeled goat anti-mouse lgG (H + L) was purchased from Zhongshan Golden Bridge Biotechnology Co. Ltd. (China); bovine serum albumin (BSA) and 3,3′,5,5′-tetramethylbenzidine (TMB) were from Xinjingke Biotechnology Co. Ltd. (China); streptavidin was from Tianjin Biotechnology Co. Ltd. (China); and 96-well plates were purchased from Beijing Bio Dee Bio Tech Co. Ltd.

The ELISA screening was performed following the instructions provided by the supplier of the assay kits (No. 7909, Cell Signaling Technology, Inc.). An aliquot (0.12 μL) of the enzyme solution was added to 4.38 μL of DTT kinase buffer, which consists of 5 mM DTT and 240 mM HEPES (pH = 7.5), 20 mM $MgCl_2$, 20 mM $MnCl_2$, and 12 μM Na_3VO_4. Each complex was dissolved in dimethyl sulfoxide (DMSO) to give a 4 mM solution, which was diluted with 0.05% Tween-20 in deionized water to give a 40 μM solution. The ATP/peptide mixture was prepared by addition of 0.36 μL of 10 mM ATP to 4.5 μL of 6 μM substrate peptide and then diluted with D_2O to 9 μL.

Each well of a microtiter plate was coated with 100 μL of 10 μg mL^{-1} streptavidin in carbonate−bicarbonate buffer, incubated overnight at 277 K, and then blocked with 1.5% BSA in PBS/T (PBS solution contained 0.05% Tween-20) at 310 K for 2 h, followed by three washings with PBS/T prior to use.

Various concentrations of tested complexes (4.5 μL) with 1% DMSO were added to 4.36 μL of DTT/buffer and 0.12 μL of 188 ng μL^{-1} EGFR and incubated at 298 K for 5 min, followed by addition of the mixture of 0.45 μL of PTP1B (Tyr66), 0.36 μL of ATP, and 4.14 μL of D_2O, and then the resulting mixture was incubated at 310 K for 1 h. The phosphorylation reaction was terminated by the addition of 18 μL/well stop buffer (50 mM EDTA, pH = 8). Then, 25 μL/well of each enzymatic reaction mixture and 75 μL/well of D_2O were added to the plate (in triplicate) for incubation at 310 K for 1 h. Following three washings with PBS/T, 100 μL of primary antibody (P Tyr-100, 1:1000 in PBS/T with 1.5% BSA) was added to each well, and the plate was incubated at 310 K for another 1 h. The plate was again washed three times with PBS/T, and then 100 μL of secondary antibody (HRP-labeled goat anti-mouse lgG, 1:1000 in PBS/T with 1.5% BSA) was added to each well for 1 h of incubation at 310 K, followed by three washings with PBS/T. Finally, 100 μL of TMB substrate (TMB (1 mg mL^{-1}): citric acid-dibasic sodium phosphate buffer (pH = 5.0):30% H_2O_2 = 100:900:1) was added to each well, the plate was incubated at 310 K for 15 min, then the reaction was stopped by addition of 100 μL of 2 M H_2SO_4 to each well, and the plate was read on the ELISA plate reader (SpectraMax M5Molecular Devices Corporation) at 450 nm to determine the OD values.

Confocal Microscopic Analysis. A total of 1.2 × 10^5 A549 cells per well were plated in a laser scanning confocal Petri dish and grown in the absence/presence of EGF for 24 h. A 2.5 mg amount of Hoechst33342 was dissolved in 1 mL of deionized water, then diluted to 25 μg mL^{-1} by medium. After removing the cell culture medium and washing once with PBS, 1 mL of 1 μg mL^{-1} Hoechst33342 was added in the dark. After being incubated at 37 °C for 10 min, the cells were washed three times by 1 mL of PBS. The cells were maintained by colorless minimal medium. Fluorescence images were obtained by an FV1000-IX81 confocal laser scanning microscope (Olympus), at an excitation wavelength of 405 nm and emission wavelength of 425−500 nm.

Flow-Cytometry Double-Staining Assay. A549 cells were seeded at a density of 2 × 10^5 per well in a six-well plate and allowed to attach for 16 h; then the cells were maintained with the corresponding complexes at 310 K for 24 h. The supernatant was removed, and cells were detached by trypsinization after washing with PBS. The cells were transferred to FACS tubes after washing by PBS and centrifuged at 1000 rpm for 3 min. After resuspension in 0.5 mL of binding buffer, the cells were incubated with 5 μL of annexin-V conjugate for 5 min, followed by addition of 5 μL of 7-AAD in the dark prior to the FACS analysis. The FACS assays were performed on a Calibur flow cytometer (BD, Franklin Lakes, NJ, USA), of which the FL2 channel was used to record the intensity of annexin V-PE staining and the FL3 channel to record the intensity of 7-AAD staining. The data were quantified by Sell Quest software (BD).

Secondary Ion Mass Spectrometry Imaging. HeLa cells were seeded on silicon wafers at a density of 1 × 10^4 mL^{-1} in a cell culture dish in the medium solution containing 90% DMEM, 10% FBS, and 1% PS and incubated at 5% CO_2 and 37 °C with 50 μM tested ruthenium complex (**K2**, **K3**, or **K4**) for 24 h. Control cells were incubated alongside the ruthenium complex doped cells. The supernatants were removed, and cells were washed three times by ammonium acetate (150 mM, pH = 7.4). Then the cells were frozen using liquid nitrogen and transferred intermediately into an LGJ-12 lyophilizer (Beijing Songyuanhuaxing Technology Develop Co., Ltd.) for freeze-drying overnight. ToF-SIMS analysis was conducted on a ToF-SIMS V mass spectrometer (IONTOF GmbH, Munster, Germany). Dual-beam experiments were performed using a 10 keV argon cluster ion beam (Ar_n^+) as sputtering beam and a 30.0 keV Bi_3^+ beam as analysis beam. High spatial resolution images were collected by 256 × 256 pixels with the highest resolution of 500 nm over a 100 × 100 μm^2 area using a pulsed analysis beam (dc current = 200 pA, pulse width = 23 ns, and repetition rate = 5 kHz) at the center of a 300 × 300 μm^2 crater eroded by an Ar_n^+ sputtering source. The current of the Ar_n^+ was ∼2 nA with a lead-off time of 60 μs. Positive ion spectra were recorded and calibrated by H^+, CH_3^+, and $C_2H_5^+$. Signals were collected layer by layer, and images were conducted by using ION-TOF SurfaceLab software (version 6.4, ION-TOF, Münster, Germany) by combining specific slice(s). The signal intensities were displayed on a color scale, which were directly related to the level of detected ions of interest.

Cellular Uptake Studies. Complex **K4** was dissolved in DMSO to yield a 6 mM stock solution. A549 cells were seeded in a Corning cell culture dish containing 8 mL of growth medium. When the coverage was over 90%, the cells were treated with 50 μM (0.5% DMSO) of the complex at 310 K for 48 h. The cells were also incubated in intact medium (0.5% DMSO) as controls. Then the media were removed, and the cells were washed with PBS solution three times. PBS containing 0.04% EDTA (4 mL) was used to detach the cells. The combined cells were centrifuged for 2 min at 4 °C, and the cells were washed three times with 1 mL of ice-cold PBS. The suspension was divided into two parts. One part was used to analyze the metal content in the membrane proteins, and the other was used for DNA-bound ruthenium analysis. The Bestbio-Membrane protein extraction kit and TIANamp genomic DNA kit, RNase A (Tiangen Biotech (Beijing) Co., Ltd.), were used to extract the membrane proteins and nuclear fractions. The concentration of extracted proteins was determined by

DOI: 10.1021/acs.inorgchem.6b00309
Inorg. Chem. XXXX, XXX, XXX−XXX

theh BCA protein assay kit (Tiangen Biotech). The DNA concentration was determined by UV−visible spectroscopy (260 nm). The extracting solutions were digested with 20% HNO_3 by heating to 200 °C until completely dried. The solid residues were redissolved in 1% HNO_3, and ruthenium was quantified by ICP-MS. Cellular metal levels were expressed as nanomoles of Ru per milligram of protein or DNA. Results are presented as the mean of seven independent experiments and expressed as mean ± SD.

4. CONCLUSIONS

In summary, a series of Ru^{II} polypyridyl complexes tethering an EGFR-inhibiting pharmacophore, 4-anilinoquinazoline, ligand as antitumor agents have been designed, synthesized, and characterized. Quick hydrolysis of the chlorido ligands was found for the ruthenium complexes **K1**−**K4** synthesized in this work, but the EGFR-targeting groups were very stable. The in vitro antiproliferation assay against a series of EGRF-over-expressing cancer cell lines suggests that the anticancer potency of the most active complex, **K4**, is close to that of cisplatin and higher than that of gefitinib. Although complex **K5** exhibited the highest EGFR-inhibiting activity, the cancer cell proliferation inhibition activity is not as good as that of **K4**. **K4** and **K5** exhibited high affinity to DNA via strong minor groove binding and weak intercalation. Moreover, complex **K4** can induce a much higher ratio of late-stage apoptosis and necrosis for A549 cells than gefitinib. These findings demonstrate that the coupling of ruthenium polypyridyl subunits and EGFR-inhibiting 4-anilinoquinazoline ligands results in a class of highly active dual-targeting anticancer agents, providing a new strategy toward the future development of more effective multifunctional antitumor drugs.

■ ASSOCIATED CONTENT

Supporting Information

The Supporting Information is available free of charge on the ACS Publications website at DOI: 10.1021/acs.inorgchem.6b00309.

Hydrolysis chromatograms, MS spectra, dose−response inhibition curves against EGFR, and TOF-SIMS images of individual ions (PDF)

Crystallographic data (CIF)

■ AUTHOR INFORMATION

Corresponding Authors

*E-mail (Y. Zhao): yaozhao@iccas.ac.cn.

*E-mail (F. Wang): fuyi.wang@iccas.ac.cn.

Notes

The authors declare no competing financial interest.

■ ACKNOWLEDGMENTS

This work was financially supported by the National Natural Science Foundation of China (Grant Nos. 21301181, 21371006, 21135006, 21321003, 21127901, and 21275148), the "One-Three-Five Project" from the Institute of Chemistry, CAS (No. PY-2015-28), the Beijing National Laboratory for Molecular Sciences Open Foundation (No. 20140127), and the Anhui Provincial Natural Science Foundation (No. KJ2011A153).

■ REFERENCES

(1) Rosenberg, B.; VanCamp, L.; Krigas, T. *Nature* **1965**, *205*, 698−699.

(2) (a) Mjos, K. D.; Orvig, C. *Chem. Rev.* **2014**, *114* (8), 4540−4563. (b) Santini, C.; Pellei, M.; Gandin, V.; Porchia, M.; Tisato, F.; Marzano, C. *Chem. Rev.* **2014**, *114* (1), 815−862. (c) Romero-Canelón, I.; Sadler, P. J. *Inorg. Chem.* **2013**, *52* (21), 12276−12291. (d) Jakupec, M. A.; Galanski, M.; Arion, V. B.; Hartinger, C. G.; Keppler, B. K. *Dalton Trans.* **2008**, *2*, 183−194.

(3) Mendiguchia, B. S.; Pucci, D.; Mastropietro, T. F.; Ghedini, M.; Crispini, A. *Dalton Trans.* **2013**, *42* (19), 6768−6774.

(4) Liu, Z.; Romero-Canelon, I.; Habtemariam, A.; Clarkson, G. J.; Sadler, P. J. *Organometallics* **2014**, *33* (19), 5324−5333.

(5) Zhou, W.; Wang, X.; Hu, M.; Zhu, C.; Guo, Z. *Chem. Sci.* **2014**, *5* (7), 2761.

(6) Bergamo, A.; Sava, G. *Chem. Soc. Rev.* **2015**, *44* (24), 8818−8835.

(7) Clarke, M. J. The Potential of Ruthenium in Anticancer Pharmaceuticals. In *Inorganic Chemistry in Biology and Medicine*; American Chemical Society: Washington DC, 1980; Vol. *140*, pp 157−180.

(8) Groessl, M.; Reisner, E.; Hartinger, C. G.; Eichinger, R.; Semenova, O.; Timerbaev, A. R.; Jakupec, M. A.; Arion, V. B.; Keppler, B. K. *J. Med. Chem.* **2007**, *50*, 2185−2193.

(9) Ang, W. H.; Dyson, P. J. *Eur. J. Inorg. Chem.* **2006**, *2006* (20), 4003−4018.

(10) (a) Rademaker-Lakhai, J. M.; van den Bongard, D.; Pluim, D.; Beijnen, J. H.; Schellens, J. H. M. *Clin. Cancer Res.* **2004**, *10* (11), 3717−3727. (b) Hartinger, C. G.; Zorbas-Seifried, S.; Jakupec, M. A.; Kynast, B.; Zorbas, H.; Keppler, B. K. *J. Inorg. Biochem.* **2006**, *100* (5−6), 891−904.

(11) (a) Wang, F.; Chen, H.; Parsons, S.; Oswald, I. D.; Davidson, J. E.; Sadler, P. J. *Chem. - Eur. J.* **2003**, *9* (23), 5810−5820. (b) Yan, Y. K.; Melchart, M.; Habtemariam, A.; Sadler, P. J. *Chem. Commun.* **2005**, *38*, 4764−4776.

(12) Lincoln, R.; Kohler, L.; Monro, S.; Yin, H.; Stephenson, M.; Zong, R.; Chouai, A.; Dorsey, C.; Hennigar, R.; Thummel, R. P.; McFarland, S. A. *J. Am. Chem. Soc.* **2013**, *135* (45), 17161−17175.

(13) (a) Liu, X. W.; Chen, Y. D.; Li, L.; Lu, J. L.; Zhang, D. S. *Spectrochim. Acta, Part A* **2012**, *86*, 554−61. (b) Liao, G.-L.; Chen, X.; Ji, L.-N.; Chao, H. *Chem. Commun.* **2012**, *48* (87), 10781−10783.

(14) (a) Komor, A. C.; Barton, J. K. *Chem. Commun.* **2013**, *49* (35), 3617−3630. (b) Xu, W.; Zuo, J.; Wang, L.; Ji, L.; Chao, H. *Chem. Commun.* **2014**, *50* (17), 2123−2125.

(15) (a) Tan, C.; Lai, S.; Wu, S.; Hu, S.; Zhou, L.; Chen, Y.; Wang, M.; Zhu, Y.; Lian, W.; Peng, W.; Ji, L.; Xu, A. *J. Med. Chem.* **2010**, *53* (21), 7613−7624. (b) Wachter, E.; Heidary, D. K.; Howerton, B. S.; Parkin, S.; Glazer, E. C. *Chem. Commun.* **2012**, *48* (77), 9649−9651. (c) Han, B.-J.; Jiang, G.-B.; Wang, J.; Li, W.; Huang, H.-L.; Liu, Y.-J. *RSC Adv.* **2014**, *4* (77), 40899−40906. (d) Howerton, B. S.; Heidary, D. K.; Glazer, E. C. *J. Am. Chem. Soc.* **2012**, *134* (20), 8324−8327. (e) Tan, C.; Wu, S.; Lai, S.; Wang, M.; Chen, Y.; Zhou, L.; Zhu, Y.; Lian, W.; Peng, W.; Ji, L.; Xu, A. *Dalton Trans.* **2011**, *40* (34), 8611−8621.

(16) Brana, M. F.; Cacho, M.; Gradillas, A.; de Pascual-Teresa, B.; Ramos, A. *Curr. Pharm. Des.* **2001**, *7* (17), 1745−1780.

(17) (a) Rajendiran, V.; Murali, M.; Suresh, E.; Sinha, S.; Somasundaram, K.; Palaniandavar, M. *Dalton Trans.* **2008**, *1*, 148−163. (b) Pages, B. J.; Ang, D. L.; Wright, E. P.; Aldrich-Wright, J. R. *Dalton Trans.* **2015**, *44* (8), 3505−3526.

(18) (a) Klajner, M.; Hebraud, P.; Sirlin, C.; Gaiddon, C.; Harlepp, S. *J. Phys. Chem. B* **2010**, *114* (114), 7. (b) Brabec, V.; Novakova, O. *Drug Resist. Updates* **2006**, *9* (3), 111−122. (c) Singh, T. N.; Turro, C. *Inorg. Chem.* **2004**, *43* (23), 7260−7262.

(19) Friedman, A. E.; Chambron, J. C.; Sauvage, J. P.; Turro, N. J.; Barton, J. K. *J. Am. Chem. Soc.* **1990**, *112* (12), 4960−4962.

(20) (a) Mardanya, S.; Karmakar, S.; Maity, D.; Baitalik, S. *Inorg. Chem.* **2015**, *54* (2), 513−526. (b) Turro, C.; Bossmann, S. H.; Jenkins, Y.; Barton, J. K.; Turro, N. J. *J. Am. Chem. Soc.* **1995**, *117*, 9026−9032.

(21) (a) Ghosh, A.; Das, P.; Gill, M. R.; Kar, P.; Walker, M. G.; Thomas, J. A.; Das, A. *Chem. - Eur. J.* **2011**, *17* (7), 2089−2098. (b) Ji,

DOI: 10.1021/acs.inorgchem.6b00309
Inorg. Chem. XXXX, XXX, XXX−XXX

L.-N.; Zou, X.-H.; Liu, J.-G. *Coord. Chem. Rev.* **2001**, *216*−*217*, 513−536.
(22) Moscatello, D. K.; Holgado-Madruga, M.; Godwin, A. K.; Ramirez, G.; Gunn, G.; Zoltick, P. W.; Biegel, J. A.; Hayes, R. L.; Wong, A. J. *Cancer Res.* **1995**, *55* (23), 5536−5539.
(23) Ogiso, H.; Ishitani, R.; Nureki, O.; Fukai, S.; Yamanaka, M.; Kim, J.-H.; Saito, K.; Sakamoto, A.; Inoue, M.; Shirouzu, M.; Yokoyama, S. *Cell* **2002**, *110* (6), 775−787.
(24) Ullrich, A.; Coussens, L.; Hayflick, J. S.; Dull, T. J.; Gray, A.; Tam, A. W.; Lee, J.; Yarden, Y.; Libermann, T. A.; Schlessinger, J.; Downward, J.; Mayes, E. L. V.; Whittle, N.; Waterfield, M. D.; Seeburg, P. H. *Nature* **1984**, *309* (5967), 418−425.
(25) Cohen, P. *Nat. Rev. Drug Discovery* **2002**, *1* (4), 309−315.
(26) Muhsin, M.; Graham, J.; Kirkpatrick, P. *Nat. Rev. Drug Discovery* **2003**, *2* (7), 515−516.
(27) (a) Kurzwernhart, A.; Kandioller, W.; Bartel, C.; Bachler, S.; Trondl, R.; Muhlgassner, G.; Jakupec, M. A.; Arion, V. B.; Marko, D.; Keppler, B. K.; Hartinger, C. G. *Chem. Commun.* **2012**, *48* (40), 4839−4841. (b) Kurzwernhart, A.; Kandioller, W.; Bachler, S.; Bartel, C.; Martic, S.; Buczkowska, M.; Muhlgassner, G.; Jakupec, M. A.; Kraatz, H. B.; Bednarski, P. J.; Arion, V. B.; Marko, D.; Keppler, B. K.; Hartinger, C. G. *J. Med. Chem.* **2012**, *55* (23), 10512−10522. (c) Wang, X.; Guo, Z. *Chem. Soc. Rev.* **2013**, *42* (1), 202−224. (d) Kilpin, K. J.; Dyson, P. J. *Chem. Sci.* **2013**, *4* (4), 1410−1419.
(28) (a) Cheng, Q.; Shi, H.; Wang, H.; Min, Y.; Wang, J.; Liu, Y. *Chem. Commun.* **2014**, *50* (56), 7427−7430. (b) Pathak, R. K.; Marrache, S.; Choi, J. H.; Berding, T. B.; Dhar, S. *Angew. Chem., Int. Ed.* **2014**, *53* (7), 1963−1967.
(29) Wilhelm, S.; Carter, C.; Lynch, M.; Lowinger, T.; Dumas, J.; Smith, R. A.; Schwartz, B.; Simantov, R.; Kelley, S. *Nat. Rev. Drug Discovery* **2006**, *5* (10), 835−844.
(30) Baselga, J. *Science* **2006**, *312* (5777), 1175−1178.
(31) (a) Zheng, W.; Luo, Q.; Lin, Y.; Zhao, Y.; Wang, X.; Du, Z.; Hao, X.; Yu, Y.; Lu, S.; Ji, L.; Li, X.; Yang, L.; Wang, F. *Chem. Commun.* **2013**, *49* (87), 10224−10226. (b) Zhang, Y.; Zheng, W.; Luo, Q.; Zhao, Y.; Zhang, E.; Liu, S.; Wang, F. *Dalton Trans.* **2015**, *44* (29), 13100−13111. (c) Du, J.; Zhang, E.; Zhao, Y.; Zheng, W.; Zhang, Y.; Lin, Y.; Wang, Z.; Luo, Q.; Wu, K.; Wang, F. *Metallomics* **2015**, *7* (12), 1573−1583.
(32) Lu, S.; Zheng, W.; Ji, L.; Luo, Q.; Hao, X.; Li, X.; Wang, F. *Eur. J. Med. Chem.* **2013**, *61*, 84−94.
(33) Liu, H.-K.; Sadler, P. J. *Acc. Chem. Res.* **2011**, *44* (5), 349−359.
(34) Guan, Y.; Zhou, W.; Yao, X. H.; Zhao, M. P.; Li, Y. Z. *Anal. Chim. Acta* **2006**, *570* (1), 21−28.
(35) Sarwar, T.; Rehman, S. U.; Husain, M. A.; Ishqi, H. M.; Tabish, M. *Int. J. Biol. Macromol.* **2015**, *73*, 9−16.
(36) (a) Ono, M.; Hirata, A.; Kometani, T.; Miyagawa, M.; Ueda, S.; Kinoshita, H.; Fujii, T.; Kuwano, M. *Mol. Cancer Ther.* **2004**, *3* (4), 465−472. (b) Reddy, K. B.; Mangold, G. L.; Tandon, A. K.; Yoneda, T.; Mundy, G. R.; Zilberstein, A.; Osborne, C. K. *Cancer Res.* **1992**, *52* (13), 3636−3641.
(37) Wakeling, A. E.; Guy, S. P.; Woodburn, J. R.; Ashton, S. E.; Curry, B. J.; Barker, A. J.; Gibson, K. H. *Cancer Res.* **2002**, *62* (20), 5749−5754.
(38) (a) Sullivan, B. P.; Salmon, D. J.; Meyer, T. J. *Inorg. Chem.* **1978**, *17* (12), 3334−3341. (b) Hartshorn, R. M.; Barton, J. K. *J. Am. Chem. Soc.* **1992**, *114* (15), 5919−5925.

DOI: 10.1021/acs.inorgchem.6b00309
Inorg. Chem. XXXX, XXX, XXX−XXX